Supporting Information

A Neutron Scattering Perspective on the Structure, Softness and Dynamics of the Ligand Shell of PbS Nanocrystals in Solution

T. Seydel[1], M. M. Koza[1], O. Matsarskaia[1], A. André[2], S. Maiti[3,#], M. Weber[2], R. Schweins[1], S. Prévost[4], F. Schreiber[3,5], M. Scheele[2,5]*

[1]Institut Max von Laue - Paul Langevin (ILL), 71 Avenue des Martyrs, CS 20156, 38042 Grenoble Cedex 9, France

[2]Institute of Physical and Theoretical Chemistry, University of Tübingen, Auf der Morgenstelle 18, 72076 Tübingen, Germany.

[3]Institute of Applied Physics, University of Tübingen, Auf der Morgenstelle 10, 72076 Tübingen, Germany

[4] ESRF-- The European Synchrotron, 71 Avenue des Martyrs, CS 40220, 38043 Grenoble Cedex 9, France

[5]Center for Light-Matter Interaction, Sensors & Analytics LISA+, University of Tübingen, Auf der Morgenstelle 15, 72076 Tübingen, Germany.

*present address: Institut Max von Laue - Paul Langevin (ILL), CS20156, 38042 Grenoble, France

Present address: Institute of Neuroscience and Medicine, Forschungszentrum Jülich, 52425 Jülich, Germany

Table of Content

Methods ... 3
Synthesis of PbS/OA NCs ... 3
SANS and SAXS ... 3
Quasi-Elastic Neutron Scattering (QENS) ... 4
Inelastic Neutron Scattering (INS) by Time-of-Flight Spectroscopy (TOF) ... 4
Data Reduction and Analysis ... 5
Fitting of the QENS Data from IN16B ... 5
Analysis of the Elastic Incoherent Structure Factor ... 6
Analysis of the fixed-window data ... 7
Fitting of the QENS Data from IN5 ... 8
Analysis of SANS and SAXS Data ... 9
A Brief Introduction into Small-Angle Scattering ... 9
Model-free information obtained from SANS and SAXS data ... 9
SANS and SAXS Data Fitting ... 9
Calculation of Solvation Degree of OA shell ... 12
Scattering Length Densities ... 13
Calculation of the Scattering Power ... 13
Calculation of the concentration of free oleic acid in the NC sample ... 14
Estimation of the number of ligands to desorb from the NC surface within the measurement time window ... 14
Calculation of the volume fraction in the NC sample ... 15
Temperature-dependent redistribution of phonon modes in the NC sample ... 15
Characteristic energies in the solid and liquid states ... 16
Quasi-elastic scattering recorded on IN5 ... 18
Diffusion of pure d-hexane ... 20
References ... 21

Methods

Synthesis of PbS/OA NCs

PbS NCs are synthesized by a procedure modified from the work of Weidman *et al.*[1] 0.040 g of sulfur and 7.5 mL of OLA are filled into a 20 mL glass vial and placed on a magnetic stirrer at room temperature in a nitrogen filled glovebox overnight. 7.5 g of $PbCl_2$ and 22.5 mL of oleylamine are filled into a 100 mL three neck flask equipped with a reflux condenser, a septum and a temperature control couple. The flask is evacuated for ~ 30 minutes until the bubble formation in the liquid stops, after which the mixture is heated to 120 °C under nitrogen. Care must be taken in this step that the $PbCl_2$ powder stays well suspended in the oleylamine. 6.75 mL of the sulfur-oleylamine solution are swiftly injected. The temperature subsequently drops to ~ 100 °C, but rises to 120°C within 1-2 min. An overshoot of temperature is prevented by tuning down the thermostat shortly before reaching 120 °C. After the reaction time (typically 30 min), the mixture is rapidly cooled down by replacing the heating mantle with a water bath and injecting 60 mL of hexane. The reaction mixture is transferred to a nitrogen-filled glovebox and precipitated with ~ 80 mL ethanol. The suspension is centrifuged with 4000 rpm for 5 minutes and the supernatant is discarded. The precipitate is redispersed in ~ 80 mL hexane. There is still unreacted $PbCl_2$ in that mixture that needs to be separated from the QD solution. That is done by centrifuging it again at 4000 rpm for 5 minutes and discarding the white precipitate. The NCs are again precipitated by ~ 80 mL of ethanol and after discarding the supernatant, 4 mL of degassed oleic acid (OA, Aldrich, 90 % technical grade) are added and the mixture is stirred with a spatula. After leaving the mixture stand for minimum 1 h, it is cleaned three times by a.) adding ~ 80 mL hexane, b.) adding ~ 80 mL of ethanol, c.) centrifuging at 4000 rpm for 5 minutes and discarding the supernatant after centrifugation.

SANS and SAXS

SAXS experiments were performed on the instrument ID02 at ESRF - The European Synchrotron, Grenoble, France.[2] A CCD detector Rayonix MX170HS was used with binning 2×2 (effective square pixel size 88.34 µm corresponding also to the point-spread-function characteristic width), placed at 3 distances from the sample: 0.77, 5.00 and 30.69 m (sample offset measured with silver behenate). The wavelength was constant at 0.0990 nm (12519.0 eV as regularly verified from absorption edges of metal foils, relative fwhm 10^{-4}). The illuminated sample cross-section was about 0.4x0.6 mm² at high q and 0.25x0.4 mm² at mid and low q, with a Gaussian profile and most of the flux density on 50x150 µm². The flux was $5.5*10^{12}$ ph/s at high q and $2*10^{12}$ ph/s at mid and low q, with exposure times ranging from 30 to 250 ms. Samples were poured in quartz capillaries (WJM-Glas, Berlin, Germany) of ca. 1.5 mm pathway and 10 µm wall thickness. Data were automatically corrected with the beamline's standard workflow accounting for transmitted photons measured with a calibrated PIN diode atop the beam stop (with a known delay between fast shutter and detector acquisition), flat field, dark, spatial distortion; 2D data were azimuthally averaged. About 10 frames were averaged and the standard-deviation was used as error-bar. Intensities were corrected by the capillary thickness determined by transmission scan. The contribution from the solvent was subtracted. The absolute scale was cross-checked by comparison of the forward scattering of the solvent

and the theoretical value from isothermal compressibility and electron density and was better than 1 %.

SANS experiments were performed on the small-angle scattering instrument D11 (Institut Laue-Langevin (ILL), Grenoble, France).[3] Samples were filled into quartz cells (110-QS, Hellma, Müllheim, Germany) and the cells were placed on a temperature-controlled copper sample holder. The measurements were performed at room temperature.

The samples were measured at sample-to-detector distances of 39, 8 and 1.4 m, covering a q range from 0.0015 to 0.45 $Å^{-1}$. The incoming neutron wavelength, λ, was 6 Å with a full width-half maximum (FWHM) wavelength spread of 9%. The beam size was 7 x 10 mm^2. Scattered neutrons were detected via a ^{3}He gas detector (CERCA) with a pixel size of 3.75 x 3.75 mm^2 and a total pixel number of 256 x 256. Data were calibrated to an absolute scale using water (H_2O) scattering intensity, $d\sigma/d\Omega = 0.983$ cm^{-1} as a secondary calibration standard. Raw data were saved in the NeXus (.nxs) format.[4] Prior to further analysis, all 2D scattering profiles obtained were corrected for both transmission and background scattering

Quasi-Elastic Neutron Scattering (QENS)

QENS spectra were recorded on the IN16B and the IN5 spectrometers at the ILL and saved in the NeXus (.nxs) format.[4] The maximum energy transfer (30 µeV) and energy resolution (0.8 µeV) at IN16B are ideally suited to study diffusive processes in the range for $D = 10^{-10} – 10^{-12}$ m^2/s.[5] Full spectra (energy range -30 µeV < E < +30 µeV) were measured on IN16B at the temperatures 183K, 239K, and 295K. In addition, elastic ($\Delta E = 0$ µeV) and inelastic ($\Delta E = 1.3$ µeV) fixed window scans were recorded in the temperature range 239K<T<295K.[6] This experiment achieves a very high energy resolution by defining the incident neutron energy and determining the scattered neutron energy using Bragg scattering at perpendicular incident angles to the monochromator and analyzer single crystal surfaces. The backscattering single crystals were chosen to be Si(111), corresponding to E = 2.08 µeV, employing the cold neutron backscattering spectrometer IN16B at the ILL, achieving an energy resolution of 0.8µeV FWHM.[5]

In contrast, the energy resolution at IN5 is sufficient to resolve the QENS signal of fast relaxational dynamics, such as diffusion processes with diffusion coefficients D significantly larger than 10^{-10} m^2/s. This includes the diffusion of the d_{14}-hexane solvent. To this end, we used the Stokes and anti-Stokes lines of the INS signal acquired at IN5 as laid out below.

Inelastic Neutron Scattering (INS) by Time-of-Flight Spectroscopy (TOF)

The neutron energy loss (Stokes line) is limited to less than the incident neutron energy, which was chosen to be 3.3 meV ($\lambda = 5$ Å) at the TOF spectrometer IN5 at ILL. With this setup, we accessed an energy resolution of 80 µeV FWHM and a momentum q range of 0.3-2.5 $Å^{-1}$ at the elastic line. There is no limit to the energy gain of neutrons (anti-Stokes line), however, the signal intensity is scaled by the Bose occupation number. Thus, the signal quality is temperature-dependent.[5] All samples were measured at 100, 150, 183, 200, and 239 K. The temperatures employed in our experiment were high enough to record the inelastic response in the entire energy range of vibrational excitations of the PbS NCs, i.e. more than 35 meV. In addition, PbS/OA/d_{14}-hexane and OA/d_{14}-hexane were measured at 2 K for low-temperature

resolution and background references. A standard helium cryostat was used with He exchange gas of a pressure of about 10 mbar at 100 K for thermalization purposes.

Data Reduction and Analysis

At IN5 and IN16B, auxiliary correction measurements of empty sample holder and vanadium standard have been carried out with the sample scans. Standard data correction for background scattering, detector efficiencies comprising the energy dependence of the counter efficiencies were applied to the IN5 data. The IN5 signal recorded as a double differential cross section in the natural units of the experiment, i.e. TOF and scattering angle 2θ, was sequentially transformed into the dynamic structure factor $S(2\theta,\omega)$, with ω denoting energy, then into the GDOS(2θ,ω) and summed over spectra in the 2θ range of 50 to 130 degrees. The derived GDOS has been normalized to 60 phonon modes in the energy range 0.5-48 meV irrespective of the sample composition. This approach is justified by the negligible scattering contribution of the PbS NC in the specimen. The data were reduced with the software package lamp and the standard routines implemented therein (https://www.ill.eu/users/support-labs-infrastructure/software-scientific-tools/lamp/).

For the analysis of the IN5 QENS signal, standard reductions and the interpolation of $S(2\theta,\omega)$ onto a constant momentum q grid as $S(q,\omega)$ were carried out using the software package lamp (https://www.ill.eu/users/support-labs-infrastructure/software-scientific-tools/lamp/).

Equivalent standard reductions were carried out for the IN16B QENS data, using the software package Mantid (www.mantidproject.org). No interpolation to a constant (q,ω)-grid was required in this case due to the small energy transfers.

The QENS data from both IN16B and IN5 were subsequently fitted using the python3 scipy.optimize.curve_fit algorithm, employing the models as reported in the results section and SI.

Fitting of the QENS Data from IN16B

The OA accounts for most of the incoherent scattering reflected by the QENS signals in **Figure 2** in the main body of the manuscript. Due to the low OA concentration, these measured signals, even though well visible, are too weak to be reliably fitted for each q-value independently. For this reason, we include the q-dependence of the scattering function in our model and fit the spectra for all (q,ω) simultaneously according to the following heuristic model for the measured intensity $S(q,\omega)$:[7,8]

$$S(q,\omega) = \mathrm{R} \otimes \{\beta(q)[A_0(q)L(\gamma(q),\omega) + (1-A_0(q))L(\gamma(q)+\Gamma(q),\omega)] + \beta_{solvent}(q)L(\gamma_{solvent}(q),\omega) + \beta_\delta(q)\delta(\omega)\} + a\omega + b \quad (1),$$

where $\mathrm{R} = \mathrm{R}(q,\omega)$is the spectrometer resolution function, $L(\cdot,\sigma)$ a Lorentzian function with the half-width at half-maximum σ, $\delta(\omega)$the Dirac delta-function describing an apparent elastic contribution, and $0 \le A_0(q) \le 1$, $\gamma(q) \ge 0$, $\Gamma(q) \ge 0$, $\beta(q) \ge 0$, $\beta_\delta(\omega) \ge 0$, and $\beta_{solvent}(q) \ge 0$ are scalar fit parameters.

This model accounts for a superposition of a center-of-mass diffusion of the PbS NCs (or alternatively OA vesicles) and a superimposed - i.e. convoluted - internal diffusion of OA

decorating the NCs. The center-of-mass diffusion is associated with a line broadening of the QENS signal by width $\gamma(q)$, while the molecular diffusion is associated with the line width $\Gamma(q)$. The convolution of the two processes is implemented by the summation $\gamma(q)+\Gamma(q)$. The much faster d_{14}-hexane solvent molecule diffusion is described by the third Lorentzian contribution with the width $\gamma_{solvent}(q)$. In addition, a possible contribution from very large objects that appear immobile on the observation time scale of IN16B is accounted for by the last term containing the Dirac delta-function. This last term simultaneously accounts for any imperfect subtraction of the container signal. At the lowest q, this term may also account for the small-angle scattering from the decorated nanoparticles. Finally, the fitted model allows for an apparent sloped background, $a\omega + b$. We note that the center-of-mass diffusion represented by the broadening $\gamma(q)$ contains contributions from both translational and rotational diffusive motions due to the large momentum transfers accessed by our experiment.[7] The observed diffusive time scale, i.e. the coherence time of the experiment, corresponds to a few nanoseconds.

We fit both the PbS/OA/d_{14}-hexane and the OA/d_{14}-hexane IN16B spectra by **equation (1)**. In these fits, the parameters $\beta_{solvent}(q)$, $\gamma_{solvent}(q)$, a, and b are fixed using the results of the corresponding pure solvent d_{14}-hexane fits, with $\beta_{solvent}(q)$ being rescaled accounting for the volume excluded by the PbS. Technically, the scalar $0 \leq A_0(q) \leq 1$ is the ratio of the two Lorentzian contributions in **equation (1)**. $A_0(q)$ can be identified with the Elastic Incoherent Structure Factor (EISF) associated with the oleic acid diffusion. The EISF informs on the geometric confinement of localized, i.e. non-ergodic diffusive motions. The existence of the EISF in our fits supports the picture that the oleic acid molecules are at least partially attached to the surface of the NPs, such that the OA molecules do not explore the solvent ergodicly anymore. Since $\beta(q)$ and $\beta_{solvent}(q)$ are free fit parameters, the fit results for the linewidths $\gamma(q)$, $\Gamma(q)$, and $\gamma_{solvent}(q)$, as well as for $A_0(q)$ are not sensitive to the exact normalization of the apparent detector efficiency. Technically, the convolution $R \otimes \cdot$ is carried out by modeling R as a sum of an arbitrary number of Gaussian functions (3 in the case of IN16B, 5 for IN5). Therefore, the observable $S(q,\omega)$ can be fitted by a sum of Voigt functions.

The contribution of the d_{14}-hexane solvent manifests itself as a broad apparent background due to its fast diffusion. The independent fits to this solvent signal, resulting in $\beta_{solvent}(q)$ and $\gamma_{solvent}(q)$, are represented by dash-dotted lines. Note that the plots show binned data for better visibility, but the fits have been performed prior to binning for higher accuracy.

Analysis of the Elastic Incoherent Structure Factor

In **Figure S1**, we additionally report the Elastic Incoherent Structure Factor (EISF) $A_0(q)$ (**equation (1)**) for T=239K for the PbS/OA/d_{14}-hexane sample. The model employed for $A_0(q)$ reads

$$A_0(q) = p + (1-p)\cdot\left(b\cdot A_{3-jump}(q, 1.715) + (1-b)\cdot A_{sphere}(q,r)\right) \qquad (2),$$

where $A_{3-jump}(q,a) = \frac{1}{3}(1 + 2\cdot sin\,(x)/x)\; with\; x = q\cdot a$

and $A_{sphere}(q,R) = \left|\frac{3 \cdot j_1(qR)}{qR}\right|^2$.

Therein, the scalar parameter p denotes the fraction of immobile scatterers, b the relative scaling of the contributions from the diffusion inside a sphere and 3-site reorientational jump diffusion, respectively. We fix the 3-site reorientational jump length to a = 1.75Å corresponding to typical jump lengths associated with distances between H atoms. j_1 denotes the spherical Bessel function of the first order and kind.

The increasing value for R with decreasing temperature in the fits (**Figure S1**) indicates that the mean-free path of the oleic acid molecules increases with decreasing temperature, consistent with an increased ordering of the molecules.

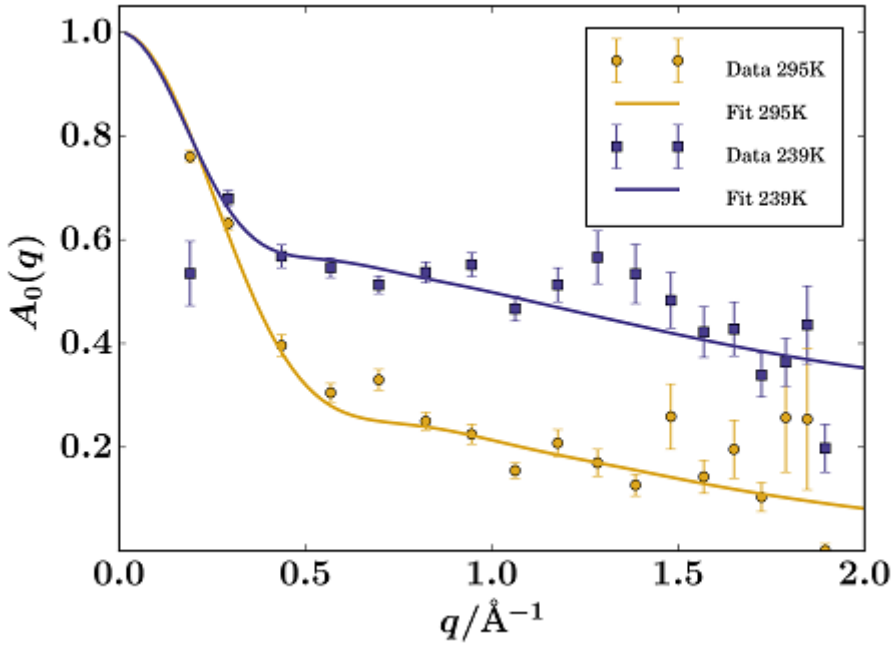

Figure S1. Elastic Incoherent Structure Factor EISF $A_0(q)$ according to **equation (1)** at T = 239 K and 295 K for PbS/OA in d_{14}-hexane obtained from the fit of the QENS spectra (symbols). Solid lines represent qualitative fits according to the heuristic model given in ref. 7,8 and **equation (2)** under the assumption of diffusion in a sphere with a smeared-out radius R=(6.5±0.4)Å for T=295 K, and R=(9.2±1.1)Å for T=239 K including a background of immobile scatterers. The errors on the symbols denote 67% confidence bounds on the fit of $A0(q)$ using **equation (1)**.

Analysis of the fixed-window data

The elastic and inelastic fixed window data give additional information on the quasi-elastic scattering by providing a much higher (quasi-continuous) temperature resolution at the expense of quantitative information on the diffusion coefficients. In addition to the results shown in the main text (**Figure 4**), a qualitative statement on the temperature-dependence of the diffusion coefficient D_1 assigned to the center-of-mass diffusion of the nanoparticles can nevertheless be obtained by plotting the ratio of the intensity measured at 1.3 μeV and at 0 μeV energy transfer, as depicted in **Figure S2**, following the procedure first applied in Ref. 9

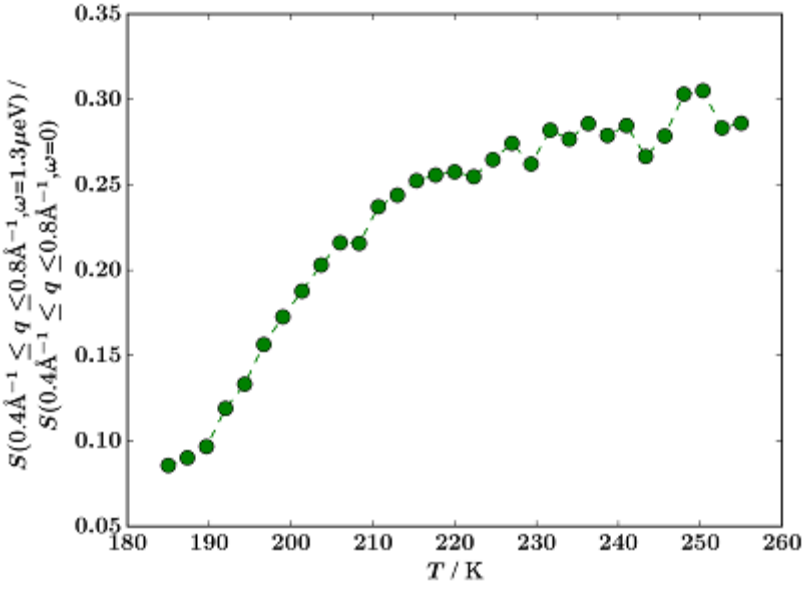

Figure S2. Ratio of the measured intensities S at 1.3 μeV and at 0 μeV energy transfer, for the PbS/OA sample, subsequent to linear interpolation to a fixed temperature grid and integration over q as given in the axis label (symbols). The monotonous increase of this ratio illustrates the presence of slow diffusive dynamics with rising temperature, which we assign to the center-of-mass diffusion of the nanocrystals.

In a simplistic picture assuming a scattering function S consisting only of a single Lorentzian function $\gamma/[\pi(\omega^2+\gamma^2)]$ without convolution with an energy resolution function, this ratio would correspond to the division of the values of this Lorentzian function taken at ω=1.3 μeV and at ω= 0 μeV, thus to $\gamma^2/(\omega^2+\gamma^2)$. For ω>>γ, the y-axis in **Figure S2** therefore directly represents the squared QENS linewidth in this simplistic approximation. Further in this simplistic picture, assuming simple Fickian diffusion $\gamma = D\,q^2$, the diffusion coefficient $D = \gamma/q^2$ could be directly obtained from such a scan. However, due to the simplifications in this approach, we abstain from a further analysis of the fixed-window data.

Fitting of the QENS Data from IN5

The model function for the quasi-elastic scattering modeled on IN5 consists of a sum of two Lorentzian functions L_1 and L_2 accounting for the solvent motions and a Dirac δ-function accounting for the apparent elastic scattering. This model is inspired by a model for pure water:[10]

$$S(q,\omega) = R(q,\omega) \otimes [I_1(q)L_1(\sigma_1(q),\omega) + I_2(q)L_2(q,\omega) + I_3(q)\delta(\omega)] \qquad (3)$$

Therein, the intensities $I_{1,2,3}$ and the Lorentzian widths $\sigma_{1,2}(q)$ are scalar fit parameters, R the spectrometer resolution function, and the ⊗-symbol denotes the convolution. As described for the IN16B QENS data, the convolution of the IN5 QENS model function with the resolution function was carried out analytically by employing Voigt functions. The EISF and nanosecond QENS signals seen on IN16B completely "disappear" within the broad resolution on IN5. Therefore, these contributions observed on IN16B are represented by the apparent elastic contribution ("Dirac" δ-function in **equation (3)**) in the model scattering function for IN5. Conversely, the broad signal from the fast solvent contribution seen on IN5 appears as an

apparent nearly flat background or very broad Lorentzian on IN16B at the limit of the accessible energy range of IN16B of 30μeV.

Analysis of SANS and SAXS Data

A Brief Introduction into Small-Angle Scattering

Generally, the angle-dependent scattered intensity, *I(q)*, obtained from a small-angle scattering experiment is approximated by the following equation, which is correct for monodisperse centro-symetrically interacting scatterers:[11]

$$I(q) \sim n \cdot P(q) \cdot S(q)$$

where $q = |\vec{q}| = \frac{4\pi}{\lambda}\sin\theta$ (with the incoming wavelength λ and the scattering angle 2θ) is the momentum transfer, n is the particle number density, ΔSLD is the contrast (scattering length density difference) between solvent and solute and V is the volume of one solute particle. The term *P(q)* is the unnormalized ($P(0) = (\Delta SLD \cdot V)^2$) form factor and represents the Fourier transform of the scattering length density of an individual particle, describing its overall shape and internal heterogeneities.[12] The term *S(q)* is the structure factor and corresponds to the Fourier transform of the pair correlation function of the system in question; it describes the net overall interactions between solute particles interacting with each other.

Model-free information obtained from SANS and SAXS data

In the case of spherical particles, their radius *R* can be determined in a model-free fashion from the minima of the *I(q)* oscillations, q_{min}, *via* the relation

$$\tan(q_{min}R) = q_{min}R$$

i.e., $q_{min} \cdot R$ = 4.49, 7.73,...[13] The radii of the PbS NCs are discussed in the main text.

SANS and SAXS Data Fitting

SANS and SAXS data were fitted with the "SASfit" software package.[14] Unless specified otherwise, all following equations are taken from the SASfit manual written by J. Kohlbrecher. The values of all fit parameters for both the SAXS and SANS data sets are listed in **Table S1**.

The **background scattering** was accounted for by the constant (q-independent) contribution I_{bkg}. It contains both the incoherent scattering due to mostly hydrogen for SANS data, and the solvent compressibility term for SANS and SAXS.

The **core-shell spherical form factor, $P_{cs}(q)$**, was used to describe oleic acid coated PbS nanoparticles. It is defined as follows:

$$P(q, R, t, SLD_c, SLD_s, SLD_0) = [K(q, R + t, SLD_s - SLD_0) + K(q, R, SLD_c - SLD_s)]^2$$

with

$$K(q, R, \Delta SLD) = \frac{4}{3}\pi R^3 \Delta SLD \cdot 3\frac{\sin qR - qR\cos qR}{(qR)^3}$$

Here, R, t, SLD_c, SLD_s, SLD_0 are the radius of the core, the shell thickness, the scattering length density of the core (index "c"), shell (index "s") and solvent (index "0").

The form factor was complemented by an ad hoc Ornstein-Zernike (OZ) contribution:

$$I_{OZ}(q) = \frac{I_{OZ}(0)}{1 + q^2\xi_{OZ}^2}$$

where ξ_{OZ} is the correlation length. This additional contribution was found necessary for SANS and SAXS data, with the same correlation length for both techniques and an intensity proportional to the contribution from all nanoparticles, and seems therefore linked to some features of these nanoparticles not accounted for by the core-shell spherical model.

A spherical **mass fractal structure factor, *S(q)*,** with exponential cut-off was used, described by the following formula:

$$S(q) = 1 + \frac{D_f}{r_0^{D_f}} \int_0^{\infty} r^{D_f - 3} h_{Exp}(r, \xi_f) \frac{\sin(qr)}{qr} r^2 dr,$$

The exponential cut-off function, $h_{Exp}(r,\xi)$ is defined *via*

$$h_{Exp}(r, \xi_f) = \exp\left[-\left(\frac{r}{\xi_f}\right)^{\alpha}\right].$$

r_0, ξ_f, D_f and α are the characteristic dimension of the individual scattering objects, the cut-off characteristic length for the fractal correlations, the fractal dimension and the exponent of the exponential cut-off function, respectively. Their respective values are given in **Table S1**. As a reminder, for the case of diffusion-limited cluster aggregates (DLCA) the fractal dimension is around 1.8 while for reaction-limited cluster aggregates (RLCA) the fractal dimension is around 2.1, and the exponent α is empirically found to be close to 2 in either case.[15]

Within a q range insensitive to the form factor and the internal structure of the system under study, the dependence of the small-angle scattering intensity on q can be expressed[16] *via* the power law

$$I(q) \sim q^{-D_f}$$

where the exponent D_f, in the case of a fractal (i.e., self-similar) system, corresponds to the so-called fractal dimension quantifying the manner in which the mass of the fractal structure increases in space.[17] D values with $3 \leq D \leq 4$ describe so-called "surface fractals", whereas $D < 3$ describes mass fractals.[18]

The SAXS data in **Figure 1** feature a power-law decay close to q^{-1}, which seemingly reflects the presence of rod-like (linear) aggregates ($D_f \approx 1$). The mass fractal fit to the SANS data, however, yields $D_f = 1.85$, i.e. SANS and SAXS (with their different contrasts towards PbS and oleic acid) apparently disagree. Given the stability of the samples, we deduce that the scattering data actually emerge from the sum of two additive and independent contributions: that of free (dispersed, non-interacting) PbS nanoparticles plus a contribution from aggregated PbS nanoparticles. The different intensity contributions for SANS and for SAXS can then be

explained by a different PbS/oleic acid ratio for free particles and for aggregated particles, with fractal aggregates depleted in oleic acid, and therefore less visible by SANS.

The model finally used is the following:

$$I(q) = I_{bkg} + I_{OZ}(q) + I_{cs,free}(q) + I_{cs,agg}(q)$$

where $I_{cs,free}(q)$ describes the contribution from non-interacting particles (no structure factor) and $I_{cs,agg}(q)$ describes the contribution of particles in fractal aggregates. The same form factor is used for both free and aggregated nanoparticles, except for the solvation of the shell that is let free. The same parameters are used to fit the SANS and SAXS data, except for the scattering length densities that are fixed to their respective known values (the shell SLD is recalculated from oleic acid and solvent SLDs based on solvation).
Qualitatively, the model describes a system sketched in **Figure S3**.

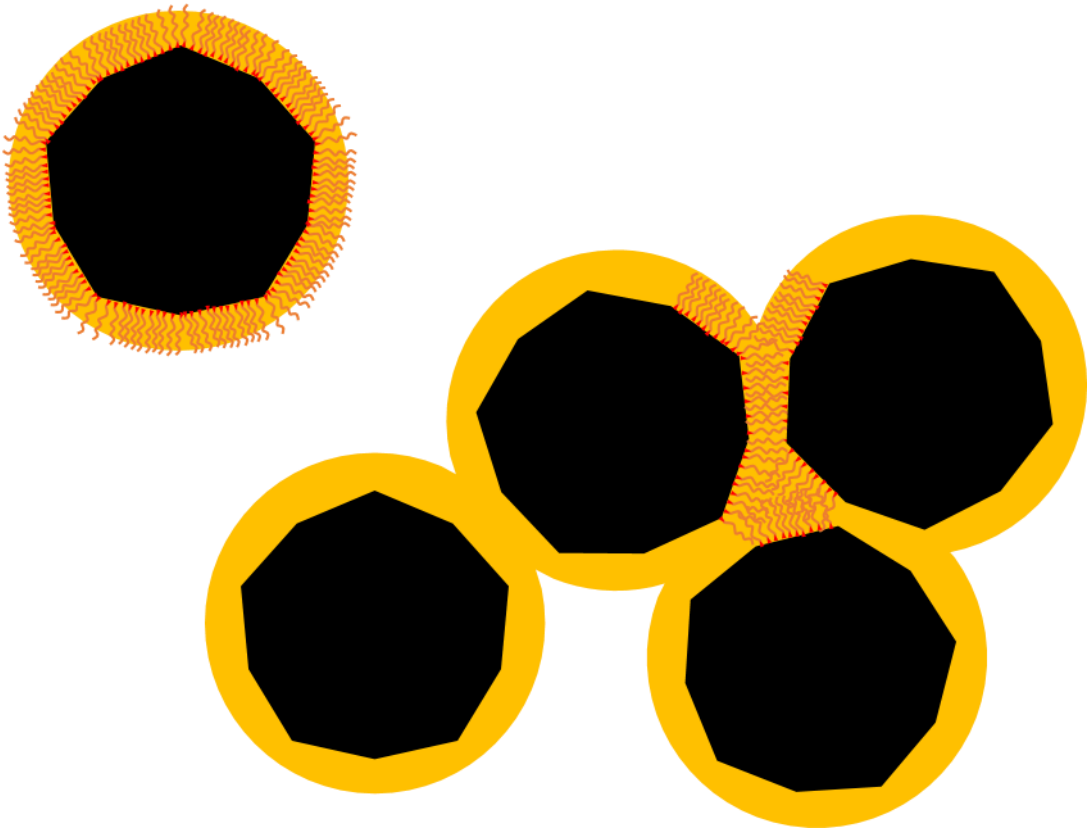

Figure S3: Illustration of the system modeled for the analysis of the SAXS data. Quasi-spherical PbS nanoparticles (black) are surrounded by an oleic-acid shell. Both free and aggregated nanoparticles are present simultaneously. The aggregated nanoparticles are depleted in oleic acid compared to the free nanoparticles, which may be justified by the sharing of oleic acid shells between neighboring particles in the fractal aggregate.

For the monomers, we calculate the degree of solvation of the OA shell to be ~80% (details of this calculation are given below). For the aggregates, we observe an OA/PbS ratio which is ~33% smaller than the one for the monomers, suggesting that the OA shells of the individual monomers overlap inside the aggregates. Whether the depletion in oleic acid for aggregated particles is a cause or a result of aggregation is unknown.

As an additional piece of information, the D_f value of 1.85 obtained from SANS indicates diffusion-limited cluster aggregation (DLCA) to be the preferential mechanism of aggregate formation.[19] This is consistent with the deviation from the expected dilute-limit Stokes-Einstein diffusion observed *via* QENS.

Table S1. Parameters obtained from SANS and SAXS fits using sasfit. (* indicates mean radius, with a log-normal distribution of relative standard-deviation 5.5 %)

		SANS	**SAXS**	
Contribution	Parameter			Unit
Background	I_{bkg}	0.047	0.024	cm^{-1}
Form factor	R	33*		Å
	t	18		Å
	ΔSLD_c	$3.8 \cdot 10^{-6}$	$-41.4 \cdot 10^{-6}$	$Å^{-2}$
	$\underline{\Delta SLD_s}$ (solvation) Dispersed NP Aggregated NP	 $4.8 \cdot 10^{-6}$ (80 %) $3.0 \cdot 10^{-6}$ (50 %)	 $-1.0 \cdot 10^{-6}$ (80 %) $-0.5 \cdot 10^{-6}$ (50 %)	$Å^{-2}$
Ornstein-Zernike	$I_{OZ}(0)$	2	5	cm^{-1}
	ξ_{OZ}	36		Å
Structure factor	r_0	35		Å
	ξ_f	310		Å
	D_f	1.85		
	α	1		
Fraction aggregated	$n_{cs,agg}/(n_{cs,agg}+n_{cs,free})$	21 %		

Calculation of Solvation Degree of OA shell

The conclusion that 80 % of the OA molecules in the shell are solvated is obtained as follows:

The theoretical neutron scattering length density difference, between d14-hexane and oleic acid is (for the respective values please see **Table S2** below)

$$SLD_{dhex} - SLD_{OA} = (6.10 \cdot 10^{-4} - 0.08 \cdot 10^{-4}) \frac{1}{Å^2} = 6.02 \cdot 10^{-4} \frac{1}{Å^2}$$

The fit to the SANS data for dispersed nanoparticles yields $SLD_s = 4.81 \cdot 10^{-4}\ \frac{1}{Å^2}$, which corresponds to ~80% of the theoretical value calculated above, thereby indicating a 20 % solvation degree of the OA shell (the SLD of the shell for SAXS also accounts for this solvation). For aggregated nanoparticles, the same calculation leads to a solvation of 50 %, i.e. the surface coverage by ligand is less for aggregated particles.

Scattering Length Densities

The scattering length densities (SLD) of the components of the system were calculated using the online tool *sld-calculator.appspot.com*. The respective values are given in **Table S2**.

Table S2. Scattering length densities of the respective system components.

Component	Density (g/cm³)	X-Ray SLD (1/ Å²)	Neutron SLD (1/ Å²)
Oleic acid ($C_{18}H_{34}O_2$)	0.895	$8.50 \cdot 10^{-6}$	$0.08 \cdot 10^{-6}$
d14-hexane (C_6D_{14})	0.763	$6.46 \cdot 10^{-6}$	$6.10 \cdot 10^{-6}$
PbS	7.6	$47.9 \cdot 10^{-6}$	$2.34 \cdot 10^{-6}$

Calculation of the Scattering Power

Concentration of H-, D- and C-atoms in pure d_{14}-hexane

With a molar weight of 100.3 g/mol and a density of 0.767 g/mL, the concentration of d_{14}-hexane in d_{14}-hexane is 7.65 mol/L. With 14 deuterium atoms per d_{14}-hexane, the concentration of D-atoms in pure d_{14}-hexane is 107.1 mol/L and the concentration of C-atoms is 45.9 mol/L. With an isotopic purity of 1 %, the concentration of H-atoms is 1.07 mol/L.

Concentration of H-, D-, C- and O-atoms in 35 mmol/L of oleic acid in d_{14}-hexane

The concentration for oleic acid of 35 mmol/L was chosen to match the concentration of bound oleic acid in the PbS/OA/d_{14}-hexane solution. With 34 H-atoms, 18 C-atoms and 2 O-atoms, this adds 1.19 mol/L H-atoms, 0.63 mol/L C-atoms, 0.07 mol/L O-atoms and 0 mol/L D-atoms to the results for pure d_{14}-hexane. The total concentrations in OA/d_{14}-hexane are therefore 107.1, 2.26, 46.5 and 0.07 mol/L for D, H, C and O, respectively.

Concentration of H-, D-, C-, O-, Pb- and S-atoms in 140 µmol/L of PbS/OA in d_{14}-hexane

There are roughly 4000 atoms in a PbS NC with a radius of 3.3 nm.[20] The excess of Pb over S-atoms (due to Pb ad-atoms in the ligand sphere) is roughly 1.3. Therefore, the concentrations of Pb and S in a 140 µL solution are 0.32 mol/L and 0.24 mol/L, respectively. Assuming a spherical particle size and a coverage of 3 OA molecules per nm^2 results in the same concentration of OA as in the previous section. Thus, the concentration of the D-, H-, C- and O-atoms is approximately the same. The total concentrations in PbS/OA/ d_{14}-hexane are 107.1, 2.26, 46.5, 0.07, 0.32 and 0.24 mol/L for D, H, C, O, Pb and S, respectively.

Multiplying these values with the total scattering cross-sections of the elements (7.6 * 10^{-24} cm^2, 82 * 10^{-24} cm^2, 5.6 * 10^{-24} cm^2, 4.2 * 10^{-24} cm^2, 11.1 * 10^{-24} cm^2 and 1.0 * 10^{-24} cm^2) yields the scattering power relevant for the time-of-flight data of all elemental components in the NC sample as shown in the **Table S3**.[21] Note that for the backscattering data only the incoherent part of the scattering cross section is to be considered.

Table S3. Relative scattering power (Rel. SP) and vibrational scattering power (vibr. SP) of the elements in the studied samples

Element	D	H	C	O	Pb	S
Rel. SP	3322	753	1048	1.2	14.5	1
Vibr. SP	53267	24134	2798	2.4	2.2	1

Figure S4 illustrates these relationships for all elements on a logarithmic scale.

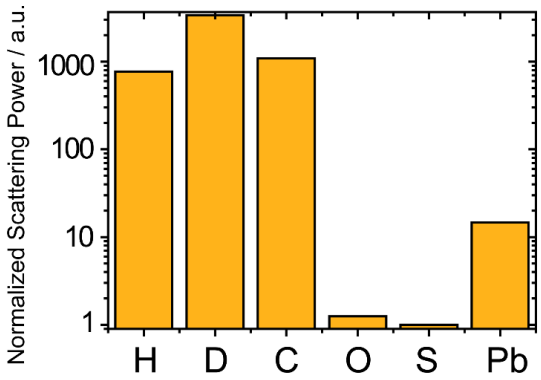

Figure S4. Relative scattering power of all elements in the sample according to the calculation in the text.

Calculation of the concentration of free oleic acid in the NC sample

Density Functional Theory calculations have shown that the binding strength of OA to the {100}-facets of PbS is relatively weak (160 meV) with an adsorption constant of 500 L/mol.[20,22,23] The density of oleic acid on the surface of the NCs is roughly 3 nm^{-2}, which results in a coverage of ~400 OA molecules per NC.[20] Based on the assumption that every second OA molecule resides on a {100}-facet and that OA molecules bound to other facets never desorb, there are 200 weakly bound OA molecules per particle. With an NC concentration of 140 µmol/L, the total concentration of exchangeable OA in the NC sample is 28 mmol/L with an adsorption constant of 500 L/mol. This corresponds to 56 µmol/L desorbed OA molecules in the sample. Thus, there are approximately three NCs per desorbed OA molecule at any time. This explains why we also observe the expected diffusion coefficient of free OA in the NC sample (D_2).

Estimation of the number of ligands to desorb from the NC surface within the measurement time window

Assuming that ligand desorption follows first order kinetics, the desorption rate is

$$v_{des} = k_{des} \cdot [OA_{bound}]$$

We infer an estimate for k_{des} from previous studies on the rate of desorption for amine-stabilized CdSe NCs in solution as (10^{-2} – 10^{-4}) s^{-1}.[24,25] As shown above, $[OA_{bound}]$ = 28 mmol/L, under the assumption that only OA molecules bound to 100 facets desorb into the liquid phase. Thus, we estimate $v_{des} = (3 \cdot 10^{-4} - 3 \cdot 10^{-6}) molL^{-1}s^{-1}$.

Considering that the sample volume investigated during a QENS experiment is roughly 1 mL and the integration time per measurement is on the order of 1 ns, this allows us to gauche the total number of desorbed OA molecules in the sample during a single measurement as

$$N = N_A \cdot (3 \cdot 10^{-4} - 3 \cdot 10^{-6}) molL^{-1}s^{-1} \cdot 10^{-3}L \cdot 10^{-9}s = 2 \cdot 10^{8} - 2 \cdot 10^{6}$$

Calculation of the volume fraction in the NC sample

The total volume of a PbS NC with 3.3 nm radius and the density of PbS (7.6 g/cm^3) is 150 nm^3. The volume of the ligand sphere can be approximated from its width of 1.8 nm (**Figure 1**) and a van-der-Waals radius of the backbone of roughly 2.5 Å, which gives 0.1 nm^3. With ~400 OA molecules per NC (see previous section), the volume occupied by the ligand sphere is 40 nm^3 and, thus, the total volume occupied by the NC and its ligand sphere is 190 nm^3. One liter of the NC solution contains 140 µmol of particles, which occupy 16 mL. The volume fraction is therefore 1.6 %.

Temperature-dependent redistribution of phonon modes in the NC sample

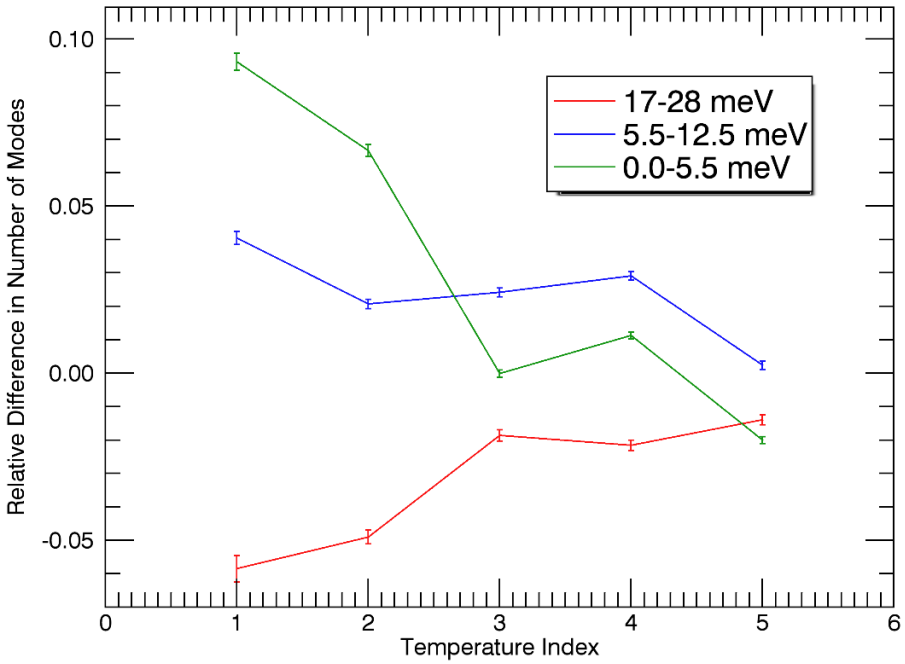

Figure S5. Temperature dependence of the relative difference in the number of phonon modes for PbS/OA/d_{14}-hexane. The temperature index on the x-axis is: (1) 100 K, (2) 150 K, (3) 183 K, (4) 200 K and (5) 239 K. Phonon modes are binned into the three energy regimes indicated in green, blue and red color. See also **Figures 5c-d** in the main part for further details.

The redistribution of modes upon heating is indicated by the relative difference in the number of modes (RDNM, **Figure S5**). The RDNM has been calculated for three energy intervals with the most significant features observed in the low and high energy ranges (0-5.5meV, 5.5-12.5 meV and 17-28 meV; see **Figure 5c-d** in the main part). At 100 K, the excess of modes is as high as 10% and 6% in the regime with lowest and highest energy, respectively. Upon heating, the RDNM approach zero, indicating the decoupling of the OA/d_{14}-hexane dynamics from the NCs and hence closer matchable spectral distributions of the solvent with and without NCs. The intermediate energy range displays a less characteristic behavior as both positive and negative intensity contributions merge with increasing T.

Characteristic energies in the solid and liquid states

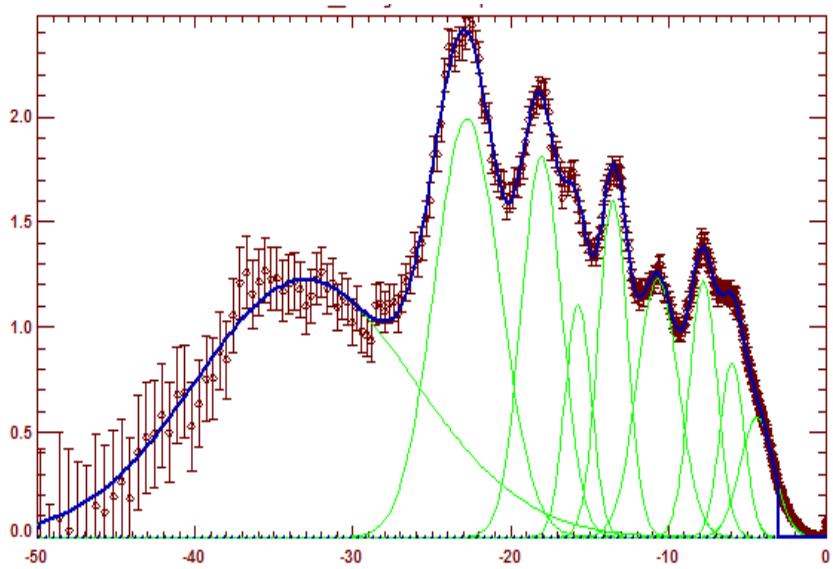

Figure S6. GDOS of d_{14}-hexane at 100 K. Solid lines correspond to Gaussian fits to the characteristic mode peaks.

The addition of OA and nano-PbS/OA to d_{14}-hexane modifies the peak intensities, enhancing particularly the modes in the low-energy range. However, the energies of the characteristic peaks are not altered. We conclude that the mixed specimens crystallize in a structure reminiscent of crystalline d_{14}-hexane. To quantify these observations, we approximate the densities of states with a set of Gaussians and list the characteristic energies derived at 100 K and 183 K in **Table S4** and **Table S5**, respectively. The fit quality is indicated in **Figure S6** reporting the set of Gaussians fitted to the GDOS of d_{14}-hexane. We find a very good match of the fitted energies with literature data exploiting other spectroscopic techniques.[26,27] Thus, we may safely state that at energies lower than 12 meV (~100 cm^{-1}), the mode peaks are exclusively due to collective lattice modes of the nanocrystals. At higher energies, a discrimination between collective lattice and intra-molecular vibrations is made difficult as both signals overlap. The approximation of the few characteristic features in the GDOS of the liquid samples results in energy parameters in agreement with literature data for intra-molecular vibrations. The enhanced variance of the results between the different specimens is the result of the reduced distinctiveness of the features. Its significance has to be taken with care.

TABLE S4: Characteristic energies of the three specimens derived from Gaussian fits to the GDOS data at 100 K, i.e. in the frozen state of d_{14}-hexane. The energy and their reliability parameters are reported in cm^{-1} for convenient comparison with literature data.

PbS/OA/dH **[cm^{-1}]**	**OA/dH** **[cm^{-1}]**	**dH** **[cm^{-1}]**
32.8 ± 1.4	34.0 ± 0.2	33.9 ± 0.4
49.1 ± 0.3	48.6 ± 0.1	48.2 ± 0.3
63.6 ± 0.3	63.6 ± 0.1	63.2 ± 0.2
85.2 ± 0.2	86.0 ± 0.1	86.1 ± 0.3
109.4 ± 0.2	108.6 ± 0.1	109.1 ± 0.3
128.2 ± 0.3	127.6 ± 0.2	126.7 ± 0.4
147.8 ± 0.4	147.9 ± 0.2	145.6 ± 0.4
183.2 ± 0.2	184.8 ± 0.1	183.6 ± 0.4
264.0 ± 1.0	262.9 ± 0.6	266.3 ± 2.4
293.1 ± 3.2	296.9 ± 1.6	
338.5 ± 2.1	333.7 ± 2.9	

TABLE S5: Characteristic energies of the three specimens derived from Gaussian fits to the GDOS data at 183 K, i.e. above the liquidus temperature of d_{14}-hexane. The energy and their reliability parameters are reported in cm^{-1} for convenient comparison with literature data.

PbS/OA/dH [cm^{-1}]	OA/dH [cm^{-1}]	dH [cm^{-1}]
135.3 ± 0.2	135.3 ± 0.8	140.7 ± 1.1
165.2 ± 1.4	160.9 ± 5.2	165.3 ± 1.2
176.5 ± 0.2	182.7 ± 0.9	184.9 ± 1.3
224.4 ± 0.5	238.4 ± 1.1	235.6 ± 2.6
290.7 ± 0.4	287.0 ± 1.1	291.8 ± 1.3

Quasi-elastic scattering recorded on IN5

Due to the large sample container diameter (22mm), the container deteriorates the resolution (**Figure S7a**). **Figure S7b** depicts an example fit of a QENS signal on IN5 for a sample containing PbS nanoparticles and oleic acid in the d-hexane solvent, at T=239K, for one example q-value. No q-dependence was imposed on the fits for the IN5 QENS data. The resulting fit parameters are according to **equation (3)** and shown in **Figures S7c-f and Figure S8**. The fits for the two Lorentzian contributions seen on IN5 result in one narrow contribution at the limit of the range visible on IN16B (**Figure S7c**) and one broad contribution far beyond the range of IN16B (**Figure S7d**). The impact of the NCs on the solvent appears to be small within the accuracy of the data and fits at least at low q-values. The effect is more notable at high q, where, however, the associated intensities of the first Lorentzian decrease. Overall, this small effect of the presence of the NCs is probably due to the depletion of the oleic acid from the solvent in the presence of the NCs. In this picture, the solvent dynamics is slightly altered by the amount of free oleic acid.

Due to the coherent scattering from the solvent (d_{14}-hexane component), a maximum of the Lorentzian intensities can be observed near or slightly above q^2=2Å^{-2} (**Figures S7c+d**). This peak appears to shift to higher q at lower temperatures, as expected.

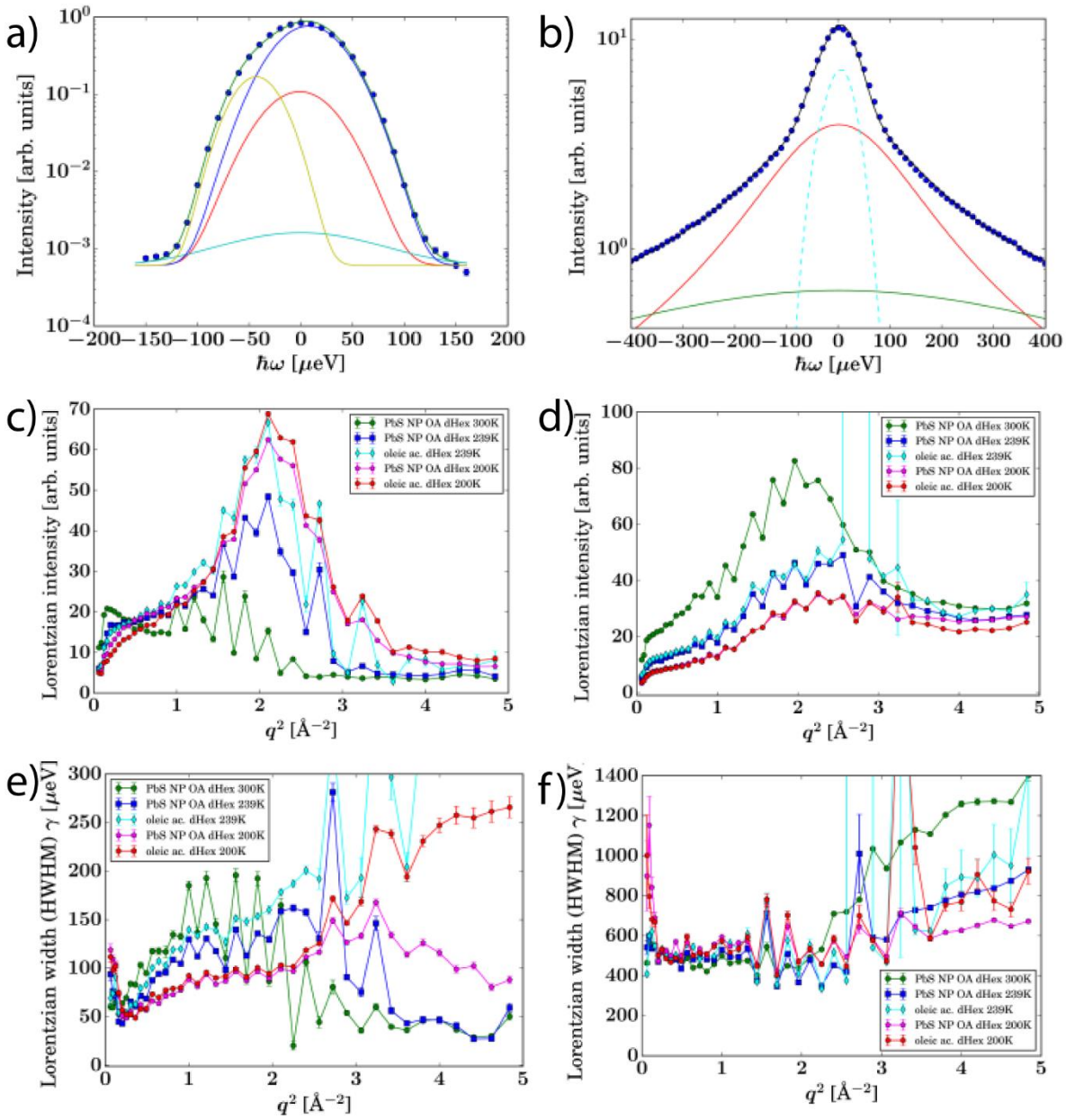

Figure S7. a) Energy resolution of IN5 measured using a Vanadium foil in the same geometry as the sample (symbols) and fit (green line superimposed on the symbols) consisting of a sum of four Gaussians (lines). Example for q=0.75Å^{-1}. **b)** Example spectrum (symbols) and fit (black line) of an IN5 QENS spectrum at q=1.0Å^{-1} and T=239K of PbS NCs/OA/d_{14}-hexane. The red and green lines represent the Lorentzians L_1 and L_2 in **equation (3)**, and the cyan dashed line denotes the apparent elastic ("Dirac") contribution. **c)** Intensity I_1 (q), **d)** Intensity I_2 (q), **e)** width σ_1 (q), and **f)** width σ_2 (q) of the two Lorentzians L_1 and L_2, which represent the solvent contributions.

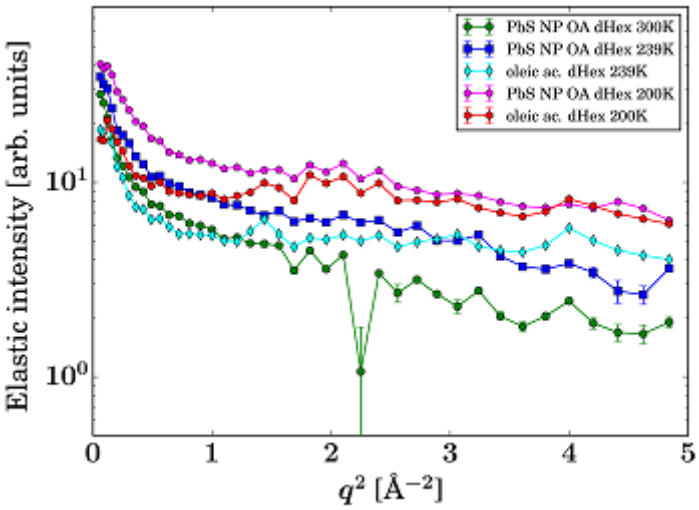

Figure S8. Apparent elastic contribution I_3 in **equation (3)** ("Dirac" δ-function) representing the immobile and slow QENS contributions much slower than the discernable motions within the energy resolution of IN5.

The apparent elastic contribution seen on IN5 (**Figure S8**) is consistent with the picture resulting from the IN16B fits: The elastic contribution is higher in the presence of the nanoparticles due to the immobile and slowly diffusing oleic acid bound to the NCs. The elastic contribution decreases with rising temperature.

Diffusion of pure d-hexane

With the IN5 data, we also obtain some information on the diffusion of pure d_{14}-hexane. Due to the strong coherent scattering, these data are difficult to interpret. Nevertheless, by fitting the low-q region of the QENS data from IN5 using the jump diffusion model, we obtain diffusion coefficients for T = 200 K and 239 K for pure d_{14}-hexane as D = (2.50±0.24) * 10^{-9} m^2/s and D = (3.03±0.33) * 10^{-9} m^2/s, respectively (**Figure S9**). In contrast, for higher temperatures, the dynamics of pure d_{14}-hexane becomes too fast even on IN5 for reliable fits of the low-q region.

These results can be compared with the diffusion coefficient D_2 obtained for the internal/confined diffusion contribution of the oleic acid. Here we obtain D_2 = (9.17±0.38) * 10^{-10} m^2/s in the presence of the nanoparticles, and D_2'=(6.51±0.19)*10^{-10} m^2/s for the diffusion inside the oleic acid vesicles in the absence of nanocrystals, respectively, at T = 239 K from the fits of the IN16B data (**Figure 3** in the main text). Thus, we conclude that the contributions of d_{14}-hexane and oleic acid can be reliably distinguished.

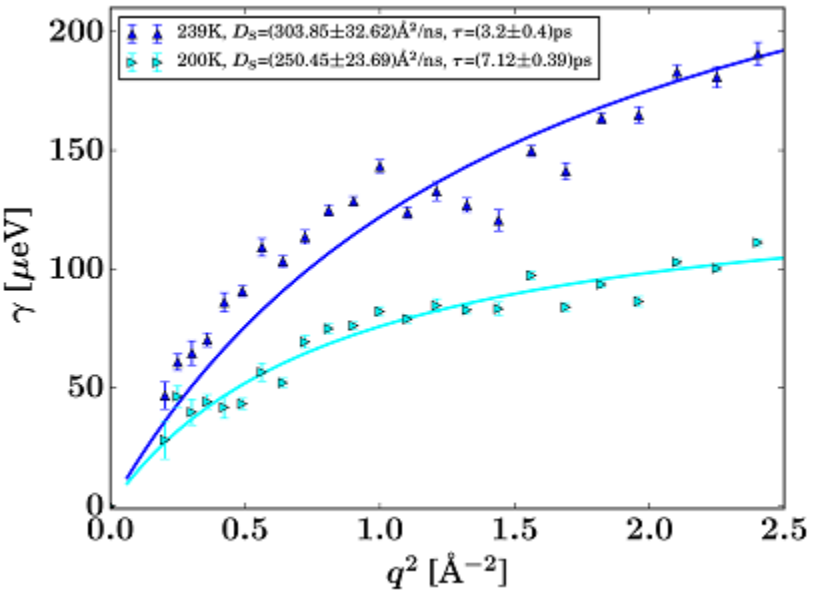

Figure S9. Linewidth (symbols) γ of the 1st Lorentzian in a fit of a sum of two Lorentzian functions to the IN5 QENS scattering signal from pure d-hexane.[10] The lines denote fits of the jump-diffusion model $\gamma(q)=D_s\ q^2/(1+D_s\ q^2\ \tau)$ with the jump diffusion coefficient D_s and the residence time τ. The fit results are reported in the legend.

References

(1) Weidman, M. C.; Beck, M. E.; Hoffman, R. S.; Prins, F.; Tisdale, W. A. *ACS Nano* **2014**, *8*, 6363–6371.

(2) Narayanan, T.; Sztucki, M.; van Vaerenbergh, P.; Léonardon, J.; Gorini, J.; Claustre, L.; Sever, F.; Morse, J.; Boesecke, P. *J. Appl. Cryst.* **2018**, *51*, 1511–1524.

(3) Lieutenant, K.; Lindner, P.; Gahler, R. *J. Appl. Cryst.* **2007**, *40*, 1056–1063.

(4) Könnecke, M.; Akeroyd, F. A.; Bernstein, H. J.; Brewster, A. S.; Campbell, S. I.; Clausen, B.; Cottrell, S.; Hoffmann, J. U.; Jemian, P. R.; Männicke, D.*; et al. J. Appl. Cryst.* **2015**, *48*, 301–305.

(5) Frick, B.; Mamontov, E.; van Eijck, L.; Seydel, T. *Z. Phys. Chem.* **2010**, *224*, 33–60.

(6) Frick, B.; Combet, J.; van Eijck, L. *Nucl. Instrum. Meth. A* **2012**, *669*, 7–13.

(7) Grimaldo, M.; Roosen-Runge, F.; Jalarvo, N.; Zamponi, M.; Zanini, F.; Hennig, M.; Zhang, F.; Schreiber, F.; Seydel, T. *EPJ Web of Conferences* **2015**, *83*, 2005.

(8) Singwi, K. S.; Sjölander, A. *Phys. Rev.* **1960**, *119*, 863.

(9) Matsarskaia, O.; Bühl, L.; Beck, C.; Grimaldo, M.; Schweins, R.; Zhang, F.; Seydel, T.; Schreiber, F.; Roosen-Runge, F. Evolution of the structure and dynamics of bovine serum albumin introduced by thermal denaturation. *Phys. Chem. Chem. Phys.* **2020**, accepted. https://doi.org/10.1039/D0CP01857K.

(10) Qvist, J.; Schober, H.; Halle, B. *J. Chem. Phys.* **2011**, *134*, 144508.

(11) Pedersen, J. S. *Adv. Colloid Interfac.* **1997**, *70*, 171–210.

(12) Sivia, D. S. *Elementary scattering theory: For X-ray and neutron users*; Oxford Univ. Press: Oxford, 2011.

(13) P. Lindner and T. Zemb, eds., *Neutrons, X-rays and light. Scattering methods applied to soft condensed matter*, North-Holland Elsevier, Amsterdam, 1st edn., **2002**.

(14) Breßler, I.; Kohlbrecher, J.; Thünemann, A. F. *J. Appl. Cryst.* **2015**, *48*, 1587–1598.

(15) Sorensen, C. M.; Wang, G. M. *Phys. Rev. E* **1999**, *60*, 7143–7148.
(16) Teixeira, J. *J. Appl. Cryst.* **1988**, *21*, 781–785.
(17) Mircea Anitas, E. *Nanomaterials* **2019**, *9*, 648.
(18) Hammouda, B. *J. Appl. Cryst.* **2010**, *43*, 716–719.
(19) Tang, S.; Preece, J. M.; McFarlane, C. M.; Zhang, Z. *J. Colloid Interface Sci.* **2000**, *221*, 114–123.
(20) Moreels, I.; Justo, Y.; Geyter, B. de; Haustraete, K.; Martins, J. C.; Hens, Z. *ACS Nano* **2011**, *5*, 2004–2012.
(21) Sears, V. F. *Neutron News* **1992**, *3*, 26–37.
(22) Zherebetskyy, D.; Scheele, M.; Zhang, Y.; Bronstein, N.; Thompson, C.; Britt, D.; Salmeron, M.; Alivisatos, P.; Wang, L.-W. *Science* **2014**, *344*, 1380–1384.
(23) Boles, M. A.; Talapin, D. V. *Science* **2014**, *344*, 1340–1341.
(24) Ji, X.; Copenhaver, D.; Sichmeller, C.; Peng, X. *J. Am. Chem. Soc.* **2008**, *130*, 5726–5735.
(25) Bullen, C.; Mulvaney, P. *Langmuir* **2006**, *22*, 3007–3013.
(26) Braden, D. A.; Parker, S. F.; Tomkinson, J.; Hudson, B. S. *J. Chem. Phys.* **1999**, *111*, 429–437.
(27) Nelligan, W. B.; LePoire, D. J.; Brun, T. O.; Kleb, R. *J. Chem. Phys.* **1987**, *87*, 2447–2456.